Dieses Dokument ist eine Zweitveröffentlichung (Verlagsversion) /

This is a self-archiving document (published version):

Katrin Philipp, Florian Lemke, Matthias C. Wapler, Ulrike Wallrabe, Nektarios Koukourakis, Jürgen W. Czarske

Spherical aberration correction of adaptive lenses

Diese Version ist verfügbar / This version is available on:

https://nbn-resolving.org/urn:nbn:de:bsz:14-qucosa2-348785

SLUB
Wir führen Wissen.

TECHNISCHE UNIVERSITÄT DRESDEN

QUCOSA
Quality Content of Saxony

PROCEEDINGS OF SPIE

Spherical aberration correction of adaptive lenses

Katrin Philipp, Florian Lemke, Matthias C. Wapler, Ulrike Wallrabe, Nektarios Koukourakis, et al.

SPIE.

Spherical aberration correction of adaptive lenses

Katrin Philipp[a], Florian Lemke[b], Matthias C. Wapler[b], Ulrike Wallrabe[b], Nektarios Koukourakis[a], and Jürgen W. Czarske[a]

[a]Technische Universität Dresden, Germany
[b]University of Freiburg, Germany

ABSTRACT

Deformable mirrors are the standard adaptive optical elements for aberration correction in confocal microscopy. Their usage leads to increased contrast and resolution. However, these improvements are achieved at the cost of bulky optical setups. Since spherical aberrations are the dominating aberrations in confocal microscopy, it is not required to employ all degrees of freedom commonly offered by deformable mirrors.

In this contribution, we present an alternative approach for aberration correction in confocal microscopy based on a novel adaptive lens with two degrees of freedom. These lenses enable both axial scanning and aberration correction, keeping the setup simple and compact. Using digital holography, we characterize the tuning range of the focal length and the spherical aberration correction ability of the adaptive lens. The operation at fixed trajectories in terms of focal length and spherical aberrations is demonstrated and investigated in terms of reproducibility. First results indicate that such adaptive lenses are a promising approach towards high-resolution, high-speed three-dimensional microscopy.

Keywords: adaptive optics, aberration correction, digital holography

1. INTRODUCTION

Laser scanning confocal microscopy is a widely used technique for the investigation of biological specimens because of the high axial and lateral resolution. However, aberrations caused by the specimens itself lead to a degradation of the resolution. In the pioneering works of Booth et al.[1,2] , the specimen-induced aberrations were corrected using a deformable mirror leading to diffraction limited resolution and significantly improved contrast. However, correcting aberrations with an deformable mirror in optical microscopes leads to bulky setups. In contrast, adaptive lenses provide axial scanning for optical microscopes while still allowing a relative compact optical setup.[3,4] Recently, adaptive lenses with spherical tunability have been presented[5,6] that promise an alternative possibility for aberration correction. In contrast to aberration correction with a deformable mirror, adaptive lenses allow for a compact setup and simultaneous axial scanning. Since the resolution of confocal microscopes is mainly degraded due to spherical aberrations, two adequately designed degrees of freedom of the lens surface should be enough to correct aberrations while simultaneously enabling axial scanning.

In this contribution, we present an adaptive lens with two degrees of freedom based on two glass-piezos that sandwich the membrane. We characterize the ability of the lens to correct spherical aberrations with emphasis to microscopic applications. Section 2 provides a description of the lens design and an introduction to the modeling of the lens parameters, namely focal length and spherical aberration. In Section 3, the tunability of the adaptive lens in terms of refractive power and spherical aberration is determined using digital holography and the robustness of fixed trajectories is investigated.

Further author information: (Send correspondence to K.P.)
K.P.: E-mail: katrin.philipp@tu-dresden.de

2. ADAPTIVE LENS WITH SPHERICAL ABERRATION CORRECTION

2.1 Lens design

The adaptive lens consists of a $50\,\mu$m thin glass membrane, which is glued in-between two piezo rings (Fig. 1). This piezo-glass sandwich seals a fluid chamber that is filled with transparent paraffin oil. The piezo rings enable a direct deformation of the glass membrane which leads to a change of the focal length of the lens depending on the curvature of the membrane. As shown in Fig. 1, one contracting and one expanding piezo ring lead to a bending deformation with an approximately parabolic lens surface (Fig. 1 left) in comparison to two contracted rings that yield a buckling deformation with a more hyperbolic lens surface (Fig. 1 right). In this way one can not only control the focal power of the lens but as well its spherical behavior (see [6] for a more complete description of the lens and [7] for the general principle).

Figure 1. Illustration of lens curvature with one expanding and one contradicting piezo ring (bending mode, left) and both piezo rings contracting (buckling mode, right) [6].

2.2 Modeling of the lens

The refractive power and spherical aberration of the lens are described in terms of Zernike coefficients of the wavefront phase. Digital holography is used to reconstruct the wavefront of a wave propagating through the adaptive lens. The phase of the wavefront ϕ is described using Zernike polynomials

$$\phi = \sum_n \sum_{m=-n}^{n} \alpha_n^m Z_n^m. \tag{1}$$

We use the defocus Zernike coefficient α_2^0 and the primary spherical Zernike coefficient α_4^0 to describe the behavior of our lens. The corresponding normalized Zernike polynomials are

$$Z_2^0 = \sqrt{3}\left(2\rho^2 - 1\right) \qquad\qquad \text{(defocus)} \tag{2}$$

$$Z_4^0 = \sqrt{5}\left(6\rho^4 - 6\rho^2 + 1\right) \qquad\qquad \text{(primary spherical)} \tag{3}$$

The defocus coefficient α_2^0 of the Zernike polynomials is used to determine the focal length f of the lens as

$$\frac{1}{f} = 4\sqrt{3} \cdot \frac{n_1 - n_0}{n_0} \frac{\lambda \alpha_2^0}{a^2} \tag{4}$$

with the wavelength λ, the refraction indices n_0 and n_1 of the surrounding medium and the lens material, respectively, and the aperture radius a of the wavefront measuring device (see appendix 4.1 for complete deviation of (4)). The primary spherical aberration coefficient α_4^0 of the Zernike polynomials is used directly to describe the sphericity of the lens, with $\alpha_4^0 = 0$ denoting a perfectly aspheric lens, i.e. without inducing spherical aberration to a wavefront with wavelength $\lambda = 532\,$nm.

3. EXPERIMENTS AND RESULTS

After introducing the conventions and notations, we now describe how to measure the Zernike coefficients using digital holography. The holograms are recorded using a Mach-Zehnder setup in off-axis configuration (see Fig. 2). The reconstruction of the object beam wavefront $\psi = Ae^{i\phi}$ is conducted using the angular spectrum method.[8,9] The recorded hologram with intensity $H(n_x, n_y)$ is transfered to its angular spectrum with intensity $S(f_x, f_y)$ using a two-dimensional fast fourier transform (FFT).

$$S(f_x, f_y) = \frac{1}{N_x N_y} \sum_{n_x=0}^{N_x-1} \sum_{n_y=0}^{N_y-1} H(n_x, n_y) \exp\left\{2\pi i(f_x n_x \Delta x + f_y n_y \Delta y)\right\} \tag{5}$$
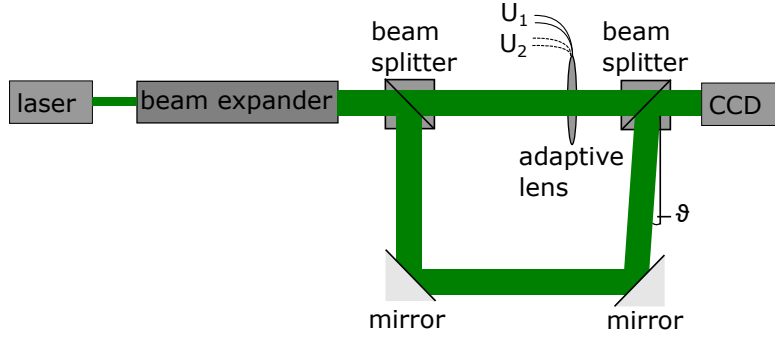
Figure 2. Mach-Zehnder setup in off-axis configuration. The laser beam of wavelength $\lambda = 532\,\text{nm}$ is expanded and split into a reference and object beam by a beam splitter. The object beam propagates through the adaptive lens and is superimposed by the reference beam at the second beam splitter with a small angle of a few degrees between the beams. The resulting hologram is recorded using a CCD camera.
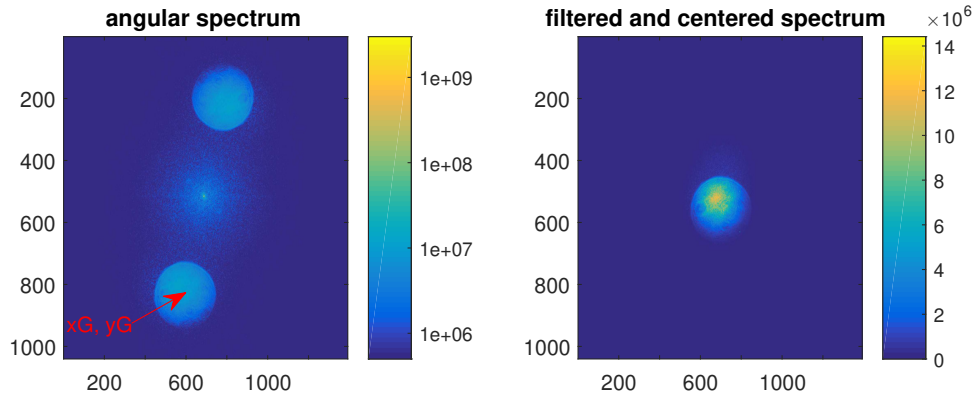

Figure 3. Left: raw angular spectrum of an adaptive lens holograph (log scale). The local maximum in the lower picture half represents the real image contribution, the central maximum the dc contribution and the maximum in the upper half is the twin-image (virtual) contribution. Right: Angular spectrum after high pass and Gaussian filtering and centered around x_G, y_G.

$H(n_x, n_y)$ is the intensity distribution of hologram at pixel position n_x, n_y, $\Delta x, \Delta y$ are the size of the camera pixels and f_x, f_y are the (digitized) angular frequencies with $f_{x/y} \in \mathbb{N}, -N_{x/y}/2 \leq f_{x,y} \leq +N_{x/y}/2$. As depicted in Fig. 3, the angular spectrum consists of a DC contribution and a contribution from the real and the virtual image. The contribution of DC-term is removed by a high-pass filter and the twin-image is eliminated by a multiplication of a Gaussian window G with the angular spectrum. The central position (x_G, y_G) of the Gaussian window is located at the center of mass of the real image contribution in the angular spectrum S. The filtered angular spectrum is then multiplied with the propagation kernel

$$K(f_x, f_y) = \exp\left\{-i\sqrt{k^2 - r^2} \cdot d\right\}, \quad r = 2\pi\sqrt{(\frac{f_x}{N_x \Delta x})^2 + (\frac{f_y}{N_y \Delta y})^2} \tag{6}$$

with the propagation distance d and the wavenumber $k = \frac{2\pi}{\lambda}$. In order to obtain the phase and amplitude of the object wave, an inverse FFT is used.

The resulting reconstructed wavefront Ψ

$$\Psi_{\text{rec}} = \frac{1}{N_x N_y} \sum_{n_x=0}^{N_x-1} \sum_{n_y=0}^{N_y-1} G(n_x, n_y) \cdot S(n_x, n_y) \cdot K(n_x, n_y) \tag{7}$$

is used to determine the phase ϕ and the amplitude A of the reconstructed wave

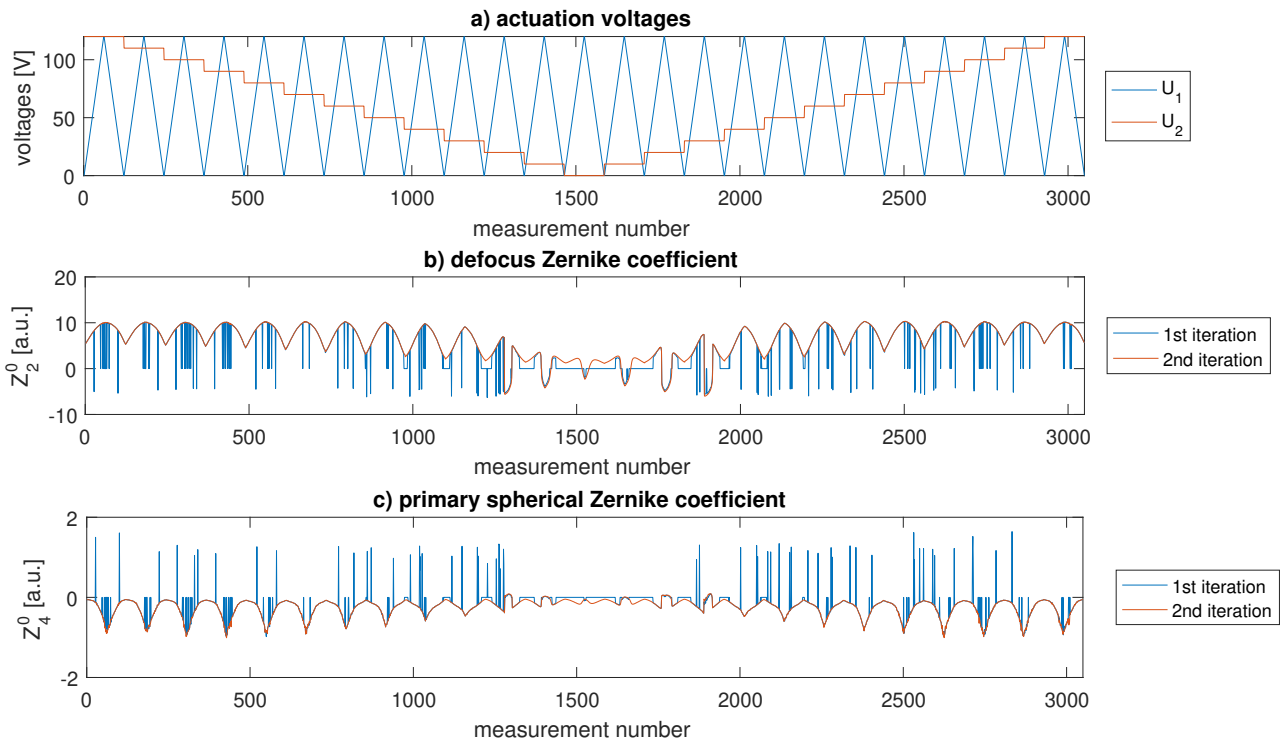$$\Psi_{\text{rec}} = A\exp\{i\phi\} \tag{8}$$

Figure 4. Actuation voltages of the two piezo rings of the adaptive lens (a), the corresponding defocus (b) and primary spherical aberration Zernike coefficients (c). 3050 different combinations of actuation voltages have been applied, denoted with the measurement number on the x-axis. The blue lines indicate the first iteration of the resulting Zernike coefficients (b+ c). The second iteration is based on the smoothed angular spectrum and phase center positions that are given to the reconstruction algorithm in order to remove the outliers in the Zernike coefficient determination (b + c, red lines).

The phase ϕ is then unwrapped using least-squares two-dimensional phase unwrapping.[10] Since the reconstruction outside the lens area is not working adequately, the reconstructed phase is cropped around its center position $(x_{\text{cent,phase}}, y_{\text{cent,phase}})$.

The defocus and spherical aberration coefficients (see Section 2.2) are now extracted from the reconstructed phase to characterize the lens behavior. For a characterization of the lens, the actuation voltages U_1 and U_2 of the two piezo rings are tuned between $0\,\text{V}$ and $120\,\text{V}$, respectively (Fig. 4). The corresponding defocus and primary spherical aberration Zernike coefficients are determined using the described digital holography evaluation. For a data evaluation that is robust against outliers of the automatically determined center position (x_G, y_G) of the Gaussian window for the filtering in the angular spectrum and the center position $(x_{\text{cent,phase}}, y_{\text{cent,phase}})$ a data evaluation consisting of two iterations is conducted. First the center positions of the Gaussian window as well of the reconstructed phase image are automatically determined. Since the actuation voltage is changed slowly and quasi-continuously with each measurement, a smooth curvature of the resulting Zernike coefficients is expected. Thus, in the second iteration, the automatically detected center positions in dependency of the measurement number are smoothed. The outliers, i.e. the center positions not laying on the smoothed curves are re-evaluated with fixed center positions. As can be seen in Fig. 4b and Fig. 4c, the second iteration yields a robust data evaluation.

By evaluating all measured combinations of actuation voltages, we determine the range of the aberration correcting adaptive lens in terms of refractive power $1/f$ and primary spherical aberration coefficient α_2^0 (Fig. 5). The lens can be operated with refractive powers between about $-3\,\text{Dpt}$ and $5\,\text{Dpt}$. As depicted in Fig. 5, spherical aberration correction Zernike coefficients in the range between about -1 and 0.1 were measured with our
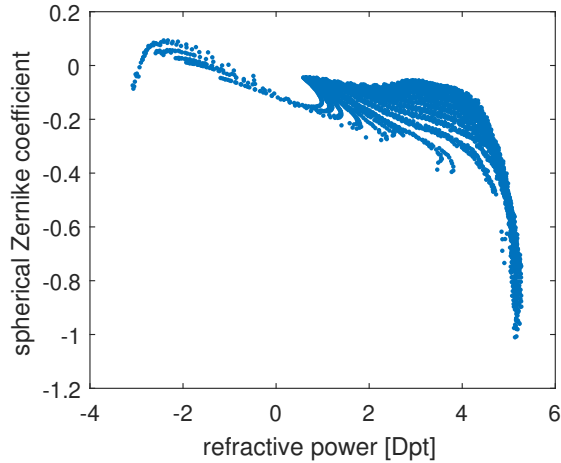
Figure 5. Spherical aberration tunability α_2^0 in dependence of the refractive power $1/f$ of the adaptive lens based on the 2nd iteration of the Zernike coefficient determination (see Figs. 4b and 4c , red lines).
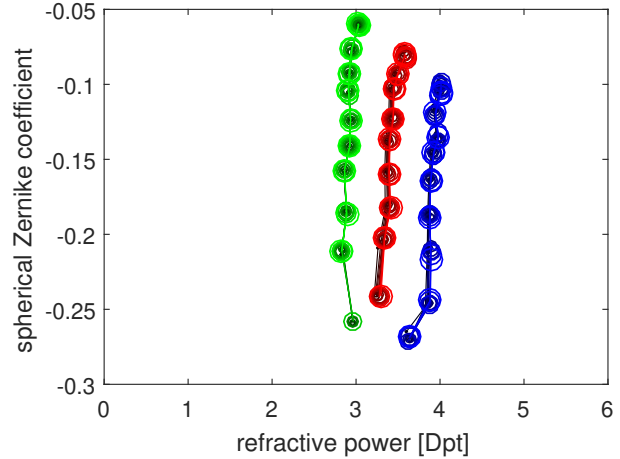
Figure 6. Tuning the spherical aberration at fixed defocus of about 2.9 Dpt(green) 3.4 Dpt(red) 3.9 Dpt(blue). The measurement was repeated ten times, the iteration number is indicated with an increasing marker size.

actuation voltages routine. The range between 1 Dpt and 4.5 Dpt promises best aberration correction capabilities because the spherical aberration Zernike coefficients can be tuned between about -0.3 and 0 in this range. Thus, the following investigates are conducted in this range.

In order to apply the adaptive lens for aberration correction in an optical microscope, the spherical aberration has to be tuned at a fixed focal length. As a proof of principle, a look-up-table for focal length and spherical aberration coefficient in dependence of the actuation voltages and voltage tuning direction has been determined. The inverted look-up-table was used to generate actuation voltage trajectories to tune the spherical aberrations at a fixed focal length as demonstrated in Fig. 6. Repeating the measurements ten times showed a mean refractive power standard deviation of $\sigma_{1/f,rel} = 0.3\,\%$ and a mean spherical aberration coefficient standard deviation of $\sigma_{Z_4^0} = 1.1\,\%$. Consequently, the aberration correcting lens promises a robust compensation for induced aberrations in a range complementary to the lens domain shown in Fig. 5. First experiments with an oko 37 channel deformable mirror that was used to introduce spherical aberrations suggest that the lens is able to correct these aberrations. Future efforts will focus on modeling of specimen-induced aberrations and their correction using the adaptive lens.

4. CONCLUSIONS

In this contribution, we presented a first investigation of the domain of an aberration correcting lens in terms of refractive power vs. spherical aberration correction. The application of fixed trajectories was demonstrated with a refractive power repeatability of a mean standard deviation of 0.3 % and a spherical aberration correction repeatability of a mean standard deviation of 1.1 %. In conclusion, this first characterization of the spherical aberration correction capability of the adaptive lens looks promising and has to be investigated further.

ACKNOWLEDGMENTS

APPENDIX

4.1 Relation between defocus coefficient α_2^0 and wavefront curvature R

In this section, the relation between the Zernike Defocus coefficient and the radius of the wavefront curvature is deviated. A spherical wavefront with radius of curvature R is assumed that enters an aperture with radius a.

This resulting phase difference Δ on the optical axis at the edge of of the aperture is given by

$$\Delta = R - \sqrt{R^2 - a^2}. \tag{9}$$

Assuming a wavefront Φ, that consists only of the normalized defocus Zernike polynomial yields

$$\Phi = \alpha_2^0 Z_2^0 = \alpha_2^0 \sqrt{3}(2\rho^2 - 1) \tag{10}$$

Note, that Φ is zero for $\rho = \pm 1/\sqrt{2}$.

Normalizing (9) to an aperture of unit radius, expressing it in units of wave numbers and setting $\Delta(\rho = \pm 1/\sqrt{2}) = 0$ yields

$$\Delta = \frac{a}{\lambda}\left(\sqrt{(R/a)^2 - \rho^2} - \sqrt{(R/a)^2 - (1/\sqrt{2})^2}\right) \tag{11}$$

which can be simplified to

$$\Delta = \frac{R}{\lambda}\left(1 - \sqrt{(\rho a/R)^2} - \sqrt{1 - (a/\sqrt{2}R)^2}\right). \tag{12}$$

A Taylor expansion of quadratic terms results to

$$\Delta = \frac{R}{\lambda}\left(1 - \frac{1}{2}\left(\frac{\rho a}{R}\right)^2 - 1 + \frac{1}{2}\left(\frac{a}{\sqrt{2}R}\right)^2\right) \tag{13}$$

which simplifies to

$$\Delta = -\frac{a^2}{4\lambda R}(2\rho^2 - 1) \tag{14}$$

Finally, the radius of curvature R is obtained by equaling (9) and (10)

$$R = -\frac{a^2}{4\sqrt{3}\lambda W_2^0}. \tag{15}$$

The focal length f is then obtained using the lensemakers equation

$$\frac{1}{f} = -\frac{n_1 - n_0}{n_0}\frac{1}{R} \tag{16}$$

with the refraction indices n_0 and n_1 for the surrounding medium and the lens fluid, respectively.

REFERENCES

[1] Booth, M. J., "Adaptive optical microscopy: the ongoing quest for a perfect image," *Light: Science & Applications* **3**(4), e165 (2014).

[2] Booth, M. J., Neil, M. A. A., Juskaitis, R., and Wilson, T., "Adaptive aberration correction in a confocal microscope.," *Proceedings of the National Academy of Sciences of the United States of America* **99**, 5788–92 (apr 2002).

[3] Koukourakis, N., Finkeldey, M., Stürmer, M., Leithold, C., Gerhardt, N. C., Hofmann, M. R., Wallrabe, U., Czarske, J. W., and Fischer, A., "Axial scanning in confocal microscopy employing adaptive lenses (CAL)," *Opt. Express* **22**(5), 6025–6039 (2014).

[4] Philipp, K., Smolarski, A., Koukourakis, N., Fischer, A., Stürmer, M., Wallrabe, U., and Czarske, J. W., "Volumetric HiLo microscopy employing an electrically tunable lens," *Optics Express* **24**, 15029 (jun 2016).

[5] Mishra, K., Murade, C., Carreel, B., Roghair, I., Oh, J. M., Manukyan, G., van den Ende, D., and Mugele, F., "Optofluidic lens with tunable focal length and asphericity," *Scientific Reports* **4**, 6378 (sep 2014).

[6] Lemke, F., Stürmer, M., Wallrabe, U., and Wapler, M. C., "Topological in-plane polarized piezo actuation for compact adaptive lenses with aspherical correction," *ACTUATOR 2016, 15th International Conference on New Actuators* (2016).

[7] Wapler, M. C., Stürmer, M., and Wallrabe, U., "A compact, large-aperture tunable lens with adaptive spherical correction," *International Symposium on Optomechatronic Technologies (ISOT) 2014* , 130–133 (2014).

[8] Kim, M. K., "Principles and techniques of digital holographic microscopy," *SPIE Reviews* **1**, 018005 (apr 2010).

[9] Koukourakis, N., Abdelwahab, T., Li, M. Y., Höpfner, H., Lai, Y. W., Darakis, E., Brenner, C., Gerhardt, N. C., and Hofmann, M. R., "Photorefractive two-wave mixing for image amplification in digital holography," *Optics Express* **19**, 22004 (oct 2011).

[10] Pritt, M. and Shipman, J., "Least-squares two-dimensional phase unwrapping using FFT's," *IEEE Transactions on Geoscience and Remote Sensing* **32**, 706–708 (may 1994).